



Signal intensity ratio of draining vein on silent MR angiography as an indicator of high-flow arteriovenous shunt in brain arteriovenous malformation

Chun-Xue Wu^{1,2} · Zhen-Xiang Zang^{1,2} · Tao Hong³ · Meng-Qi Dong³ · Yi Shan^{1,2} · Zhi-Lian Zhao^{1,2} · Cheng-Bei Hou⁴ · Jie Lu^{1,2}

Received: 9 April 2021 / Revised: 26 May 2021 / Accepted: 25 June 2021 / Published online: 15 July 2021
© The Author(s) 2021

Abstract

Objectives To evaluate whether the signal intensity ratio (rSI) of the draining vein on silent MR angiography is correlated with arteriovenous (A–V) transit time on digital subtraction angiography (DSA), thereby identifying high-flow A–V shunt in brain arteriovenous malformation (BAVM), and to analyze whether the rSI and the characteristic of draining veins on silent MRA are associated with hemorrhage presentation.

Methods Eighty-one draining veins of 46 participants with BAVM (mean age 33.2 ± 16.9 years) who underwent silent MRA and DSA were evaluated retrospectively. The correlation between the rSI of the draining vein on silent MRA and A–V transit time on DSA was examined. The AUC-ROC was obtained to evaluate the performance of the rSI in determining the presence of high-flow A–V shunt. The characteristics of draining veins with the maximum rSI (rSI_{max}) were further compared between the hemorrhagic and non-hemorrhagic untreated BAVM.

Results The rSI of each draining vein on silent MRA was significantly correlated with A–V transit time from DSA ($r = -0.81, p < .001$). The AUC-ROC was 0.89 for using the rSI to determine the presence of high-flow A–V shunt. A cut-off rSI value of 1.09 yielded a sensitivity of 82.4% and a specificity of 82.8%. The draining vein with rSI_{max} and no ectasia was significantly more observed in the hemorrhagic group ($p = 0.045$).

Conclusions The rSI of the draining vein on silent MRA is significantly correlated with A–V transit time on DSA, and it can be used as an indicator of high-flow A–V shunt in BAVM.

Key Points

- The signal intensity ratio (rSI) of the draining vein on silent MRA significantly correlated with arteriovenous (A–V) transit time of brain arteriovenous malformation (BAVM) on digital subtraction angiography (DSA).
- The area under the receiver operating characteristic curve (AUC) was 0.89 for using the rSI of draining veins to determine high-flow A–V shunt.
- Draining veins with maximum rSI and no ectasia were significantly more observed in the hemorrhagic group of BAVM ($p = 0.045$).

Keywords Magnetic resonance imaging · Magnetic resonance angiography · Arteriovenous malformations · Brain

✉ Jie Lu
imaginglu@hotmail.com

¹ Department of Radiology and Nuclear Medicine, Xuanwu Hospital, Capital Medical University, 45# Changchun Street, Xicheng District, Beijing, China

² Beijing Key Laboratory of Magnetic Resonance Imaging and Brain Informatics, Beijing, China

³ Department of Neurosurgery, Xuanwu Hospital, Capital Medical University, Beijing, China

⁴ Center for Evidence-Based Medicine, Xuanwu Hospital, Capital Medical University, Beijing, China

Abbreviations

| | |
|--------------------|--|
| ASL | Arterial spin labeling |
| AUC-ROC | Area under the receiver operating characteristic curve |
| A–V shunt | Arteriovenous shunt |
| BAVM | Brain arteriovenous malformation |
| CI | Confidence interval |
| DSA | Digital subtraction angiography |
| DV | Draining vein |
| FOV | Field of view |
| ICA | Internal carotid artery |
| ICC | Intraclass correlation coefficients |
| MIP | Maximum intensity projection |
| MRA | MR angiography |
| NPV | Negative predictive value |
| PPV | Positive predictive value |
| ROI | Region of interest |
| rSI | Ratio of signal intensity |
| rSI _{max} | Maximum ratio of signal intensity |
| TOF | Time-of-flight |
| ZTE | Zero echo time |

Introduction

Brain arteriovenous malformation (BAVM) is a cerebrovascular disease in which arteries connect directly with veins without intervening capillaries [1, 2]. The main treatment modalities for BAVM include surgery, radiosurgery, and endovascular treatment [2, 3]. Previous studies have indicated that BAVM with high-flow arteriovenous (A–V) shunt are associated with increased perioperative hemorrhagic events and higher risk of incomplete obliteration [4–7]. Therefore, identification and targeted embolization of high-flow A–V shunt in BAVM are crucial in endovascular management before radiosurgery or surgical resection.

Digital subtraction angiography (DSA) is the gold standard for evaluation of high-flow A–V shunt owing to its high spatial and temporal resolution. However, DSA is an invasive examination with unelectable risks of procedure-related complications and therefore not applicable for serial follow-up examinations. Non-invasive imaging methods such as time-resolved contrast-enhanced MRA and unenhanced time-resolved phase-contrast MRA can provide hemodynamic information, yet they require injection of contrast agent or have limited temporal resolution [8–10].

Silent MR angiography is a new imaging approach based on arterial spin labeling (ASL) and zero time echo (ZTE) techniques and does not require a contrast agent [11]. Several studies have reported that silent MRA achieved better performance in depicting the nidus and draining veins of BAVM compared to time-of-flight MR angiography (TOF

MRA) [12–14]. In these studies, a portion of the draining veins of BAVM still could not be observed on silent MRA. Meanwhile, in previous studies on cerebrovascular diseases, signal loss on silent MRA was also found in vessels with slow flow [15, 16]. In ASL, the signal decreases with the transit time from the labeling plane due to T1 recovery, and this might limit slow inflow imaging on silent MRA [16]. Based on these findings, we infer that the SI of draining veins on silent MRA might potentially be associated with blood flow velocity and thereby can be used to identify high-flow A–V shunt.

In addition, some studies indicated that a BAVM hemorrhage is associated with unbalanced inflow and outflow [8, 17]. That is, inflow is rapid, whereas outflow remains unchanged or is reduced. Therefore, we assume that the relative signal intensity and the characteristic of draining veins on silent MRA can reflect the inflow and outflow characteristics respectively. Comparing their characteristics in hemorrhagic and non-hemorrhagic groups of BAVM would be helpful to explore their potential role in BAVM hemorrhage.

Therefore, our hypotheses are as follows: (1) the signal intensity (SI) ratio of the draining vein calculated by silent MRA is correlated with the arteriovenous transit time measured by DSA, and it can be used as a useful indicator of high-flow A–V shunt of BAVM, and (2) the characteristics of draining veins with the maximum rSI on silent MRA are associated with hemorrhage presentation.

Material and methods

Patients

The study protocol was approved by the Institutional Review Board of our institution. Written informed consent was obtained from all participants or their guardians at admission.

This retrospective study included 53 consecutive patients (mean age 33 years \pm 16; 28 men) diagnosed with BAVM between May 2020 and February 2021 in a single tertiary referral institution. All patients underwent both silent MRA and DSA. Patients with MRA and DSA performed more than 4 weeks apart and patients with suboptimal imaging quality were excluded. Patients with subtentorial BAVM were not included in this study.

In patients without treatment, the initial presentation was divided into hemorrhagic or non-hemorrhagic by signs of bleeding on MRI consistent with hemorrhage history.

Angiography

According to the standard protocol, DSA was performed for all the patients by the biplane system (Philips Medical

Systems; Integris V5000). During the angiography, selective injection was performed in the vertebral arteries, internal carotid, and external carotid by using a 5-F catheter through a transfemoral route. Frontal and lateral views with a frame rate of four per second were displayed, and we injected a 5–7-mL bolus of the contrast medium iopromide (Ultravist; Schering) for each shot. In addition to the conventional DSA, a 3D rotational angiography was performed using 5 s, and thin slab-maximum intensity projection (MIP) and multiplanar reconstruction images were obtained.

MRI protocol

3T MR imaging (SIGNA Premier; GE Healthcare) was performed within 4 weeks before or after DSA on all 53 patients. Patients did not receive microsurgery, endovascular treatment, or radiotherapy between MR imaging and DSA.

The conventional MR imaging protocol included axial T2WI (flip angle 8°; TR 4924 ms; TE 107.7 ms; section thickness 5.0 mm; NEX 1; bandwidth 62.50 kHz) and 3D sagittal T1 MPRAGE (flip angle 8°; TR 1000 ms; TE 2.7 ms; section thickness 1.0 mm; NEX 1; bandwidth 31.25 kHz).

The parameters of silent MRA were as follows: field of view (FOV), 20 × 20 cm; matrix, 150 × 150; flip angle, 5°; TR, 828 ms; TE, 0 ms; section thickness, 1.2 mm; NEX, 1; bandwidth, 25 kHz; and acquisition time, 6 min 59 s; and the labeling duration, 2034 ms. 3D radial sampling was applied during the readout scheme. A 48-channel head coil was used for all patients. To avoid the influence of the labeled position on the results, the lower edge of the FOV was located at the lower edge of the C2 vertebral body level in each patient.

Image analysis

DSA image analysis

On DSA, the angioarchitecture and flow pattern (A–V transit time) of BAVM was evaluated by two interventional neurosurgeons (M.D. with 5 years of experience and T.H. with 10 years of experience) in a randomized order, with discrepancies resolved by consensus. Both of them were blinded to clinical information.

A–V transit time was estimated by determining the number of DSA frames between the first depiction of the nidus and the first visualization of a vein (high-flow A–V shunt—venous drainage seen in less than two frames after nidal visualization; non-high-flow A–V shunt—venous drainage seen in two or more frames after nidal visualization) [7]. Venous ectasia and stenosis were defined as at least 50% increase or reduction in the venous diameter in any drainage vein. Venous drainage was categorized as any deep venous drainage (exclusively deep venous drainage or superficial and deep drainage) or superficial venous drainage [18]. Flow-related aneurysm was

defined as an aneurysm that lies on a pathway supplying blood flow to the BAVM [19]. The BAVM were further classified based on the Spetzler–Martin classifications by using DSA combined with conventional MRI.

Silent MRA analysis

Two neuroradiologists (C.W. and Z.Z., with 12 and 15 years of experience, respectively), blinded to the results of DSA and clinical data, independently reviewed all the conventional MR images and silent MRA images in a randomized order.

Measurements of the nidus were performed on the conventional MRI in three dimensions. The largest diameter among the three dimensions was recorded as the BAVM size. Location was classified as being in an eloquent or non-eloquent area.

A region of interest (ROI) analysis was performed on the silent MRA source images on GE AW 4.7 Workstation. We used a circular shape for all ROIs. For draining veins (DV), the closest area to the nidus was first determined on MIP images. The ROI was put on the site on silent MRA source images and did not overlap with adjacent vessels (Fig. 1). To calculate the rSI, the cavernous ICA ipsilateral to the nidus was selected as the denominator for the rSI reference, which can easily be identified and measured on axial source images (refer to Fig. 1). For replication purposes, we performed similar analyses using the raw value of the SI of draining veins (see [supplementary materials](#)). Each ROI was set to be no larger than the target vessels, and the ROI size changed according to the vessel of interest. The ROI should exactly match the diameter of the vessel of interest. Each SI value was measured as the mean of 2 ROIs. Ratios of SI (rSI) were calculated as SI-DV / SI-ICA. The maximum ratio of SI (rSI_{max}) was defined as the highest rSI of all draining veins in each patient. If the draining vein demonstrated on DSA cannot be visualized on silent MRA, the rSI was recorded as zero.

For each patient, the assessment included (1) rSI of each draining vein; (2) rSI_{max} of all the draining veins; and (3) the diameter of the draining vein with rSI_{max}.

Subsequent statistical analysis was based on the rSI values measured by the first neuroradiologist (C.W.). On DSA, the venous drainage patterns (venous ectasia, deep venous drainage, and single venous drainage) of the draining vein with rSI_{max} were recorded.

Statistical analysis

The data were analyzed by using IBM SPSS Statistics Version 22.0 (IBM). A *p* value < 0.05 was considered statistically significant. For the radiological and clinical data, patients with and without hemorrhage presentation before treatment were

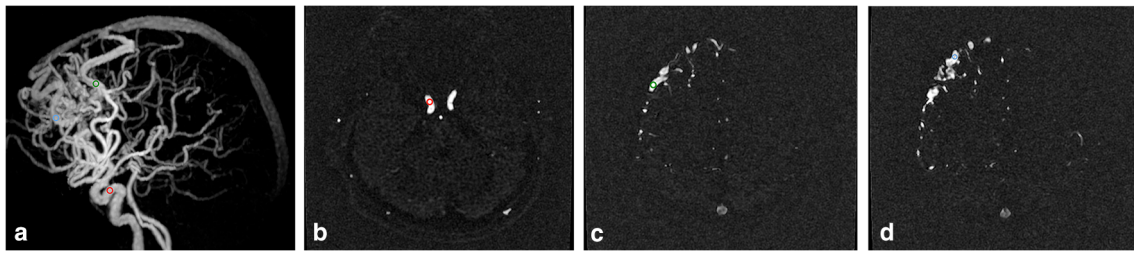


Fig. 1 **a** ROI setting on Silent MRA. **b** ROIs were set on the cavernous ICA ipsilateral to the nidus (red circle) and **(c-d)** the proximal segment of drainage veins (green and blue circle) on axial source images. The ratio of signal intensity of each draining vein was calculated.

compared using descriptive statistics. Categorical variables were evaluated using Pearson’s chi-squared test and Fisher’s test, and continuous variables were evaluated using Student’s *t* test or the Mann–Whitney *U* test when comparing the two groups.

The intraclass correlation coefficient (ICC) of the different observers was calculated to assess the reliability of the rSI measurement. ICC was categorized as follows: values < 0.4 as poor, 0.40–0.59 as fair, 0.6–0.74 as good, and ≥ 0.75 as excellent [20].

The correlations of the rSI of each draining vein and the rSI_{max} of each patient from silent MRA images with the corresponding A–V transit time from DSA were performed by Pearson correlation analysis. The same calculation was done for the correlations of rSI_{max} with the corresponding diameter of the draining vein.

The area under the receiver operating characteristic curve (AUC-ROC) was obtained to explore the performance of high-flow A–V shunt determination by the rSI from silent MRA. A point with the maximum Youden index was set as the optimal cut-off. Sensitivity, specificity, positive predictive value, and negative predictive value were calculated.

Results

Patient demographics and BAVM characteristics

Of the 53 consecutive patients, seven were excluded for the following reasons: two patients had over 4 weeks interval between silent MRA and DSA, two patients had artifacts on silent MRA images, and three patients had a nidus in the

Table 1 Characteristics of the study population

| Demographics | Total (n = 46) | Treated (n = 20) | Untreated | | <i>p</i> value |
|-----------------------|-------------------|---------------------|------------------------|----------------------------|----------------|
| | | | Hemorrhage (n = 12) | Non-hemorrhage (n = 14) | |
| Age at diagnosis (y) | 33.2 ± 16.9 | 36.6 ± 16.7 | 27.2 ± 15.6 | 33.6 ± 18.0 | 0.69 |
| Male | 25 (54.3%) | 11 (55%) | 4 (33.3%) | 10 (71.4%) | 0.11 |
| Radiological | | | | | |
| Venous drainage | | | | | |
| Single | 21 (45.7%) | 12 (60%) | 4 (33.3%) | 5 (35.7%) | 1 |
| Any deep | 12 (26.1%) | 4 (20%) | 3 (25%) | 5 (35.7%) | 0.68 |
| Venous ectasia | 33 (71.7%) | 12 (60%) | 9 (75%) | 12 (85.7%) | 0.64 |
| Deep location | 3 (6.5%) | 1 (5%) | 3 (25%) | 5 (35.7%) | 0.68 |
| Associated aneurysm | 10 (21.7%) | 1 (5%) | 6 (50%) | 3 (21.4%) | 0.22 |
| BAVM size (mm) | 31.3 ± 17.5 | 27.5 ± 16.1 | 31.6 ± 19.0 | 37.4 ± 17.7 | 0.37 |
| Spetzler–Martin grade | | | | | |
| I–II | 27 (58.7%) | 13 (65%) | 7 (58.3%) | 7 (50%) | |
| III | 13 (28.2%) | 6 (30%) | 3 (25%) | 4 (28.6%) | |
| IV–V | 6 (13.0%) | 1 (5%) | 2 (16.7%) | 3 (21.4%) | |
| High-flow A–V shunt | 15 (32.6%) | 5 (25%) | 7 (58.3%) | 3 (21.4%) | 0.11 |

Values are numbers of patients; ages are mean ± standard deviation
BAVM brain arteriovenous malformation

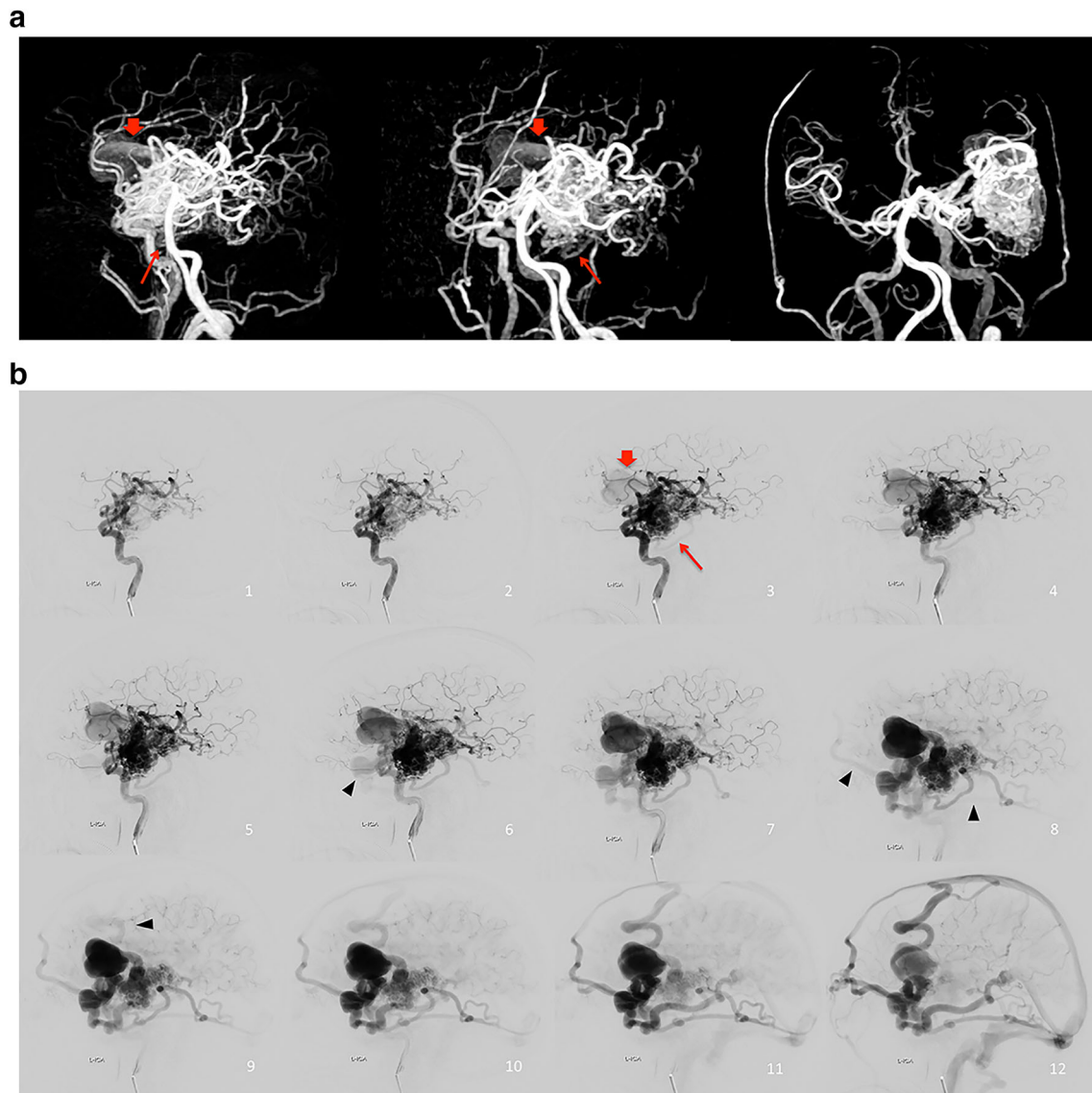


Fig. 2 Images of left temporal BAVM in a 64-year-old man, with several asynchronous draining veins toward superior sagittal, sigmoid sinus and straight sinus. **a** 3D MIP of Silent MR angiography showed one dilated draining vein (red arrow) and a small draining vein (red long arrow). **b**

Lateral view of left ICA angiography. These two veins were visualized two frames after the nidus depiction on DSA. Note that several draining veins (black arrowhead) observed more than four frames after the nidus depiction on DSA were not visible on Silent MRA.

posterior fossa. Among the 46 eligible participants, the mean age was 33.2 ± 16.9 years; range, 5–64 years; 25 men (Table 1). Twenty-six (56.5%) patients with BAVM were untreated, and 20 patients (43.5%) were previously treated by embolization and/or radiosurgery. Twenty-five patients (54.3%) had history of hemorrhage. Other symptoms (17 of 46; 37.0%) included seizure (9 of 46; 19.6%), headache (4 of 46; 8.7%), and dizziness (4 of 46; 8.7%). The BAVM was incidentally detected in 4 patients (8.7%). The mean interval between MR imaging and DSA was 5 days (range 1–15 days).

Of all 46 patients, 46 niduses and 81 draining veins (54 draining veins in the untreated group and 27 in the treated group) were detected on DSA. High-flow A–V shunt was

observed in 15 patients (10 of 26 in the untreated group and 5 of 20 in the treated group). Baseline characteristics are shown in Table 1. In patients without treatment, no significant difference was observed in any angioarchitecture features between the hemorrhagic and non-hemorrhagic groups.

Association between the rSI on silent MRA and flow pattern

All 46 niduses seen on DSA were detected on silent MRA. For all 81 draining veins, 73 (90.1%) (51 of 54 in the untreated group and 22 of 27 in the treated group) were detected on silent MRA. Five of these missing draining veins were toward

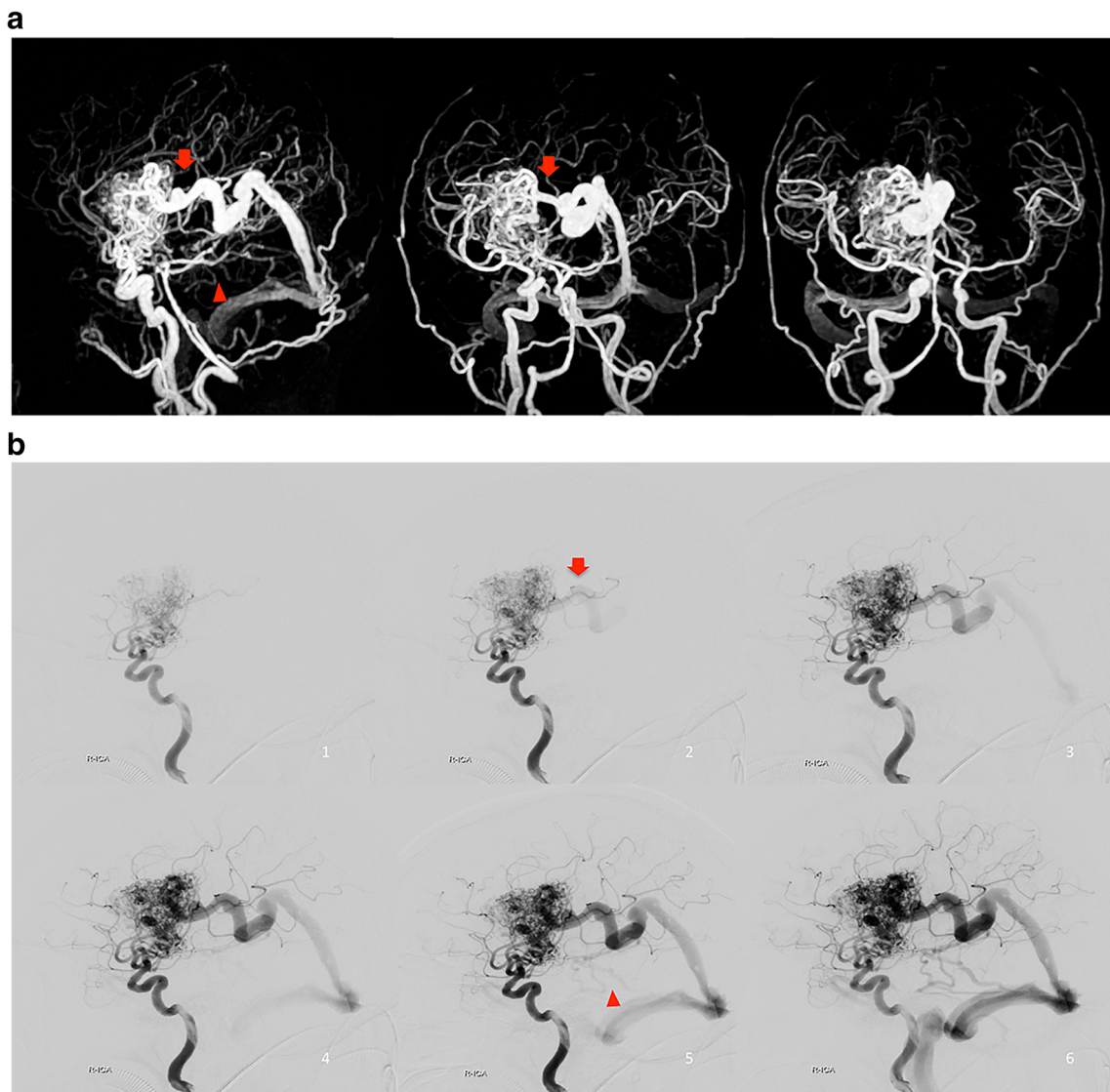


Fig. 3 Images of right basal ganglia BAVM in a 33-year-old woman, with several asynchronous draining veins toward sigmoid sinus and straight sinus. **a** 3D MIP of Silent MR angiography showed one deep draining vein with higher signal intensity (red arrow) and several small draining veins with lower signal intensity (arrowhead). **b** Lateral view of

right ICA angiography. The deep draining vein (red arrow) was visualized at the same time as one frame after the nidus depiction on DSA. The small draining veins with lower signal intensity on Silent MRA (arrowhead) were observed four frames after the nidus depiction on DSA.

Fig. 4 rSI versus arteriovenous transit time (**a**, rSI of each draining vein; **b**, rSI_{max})

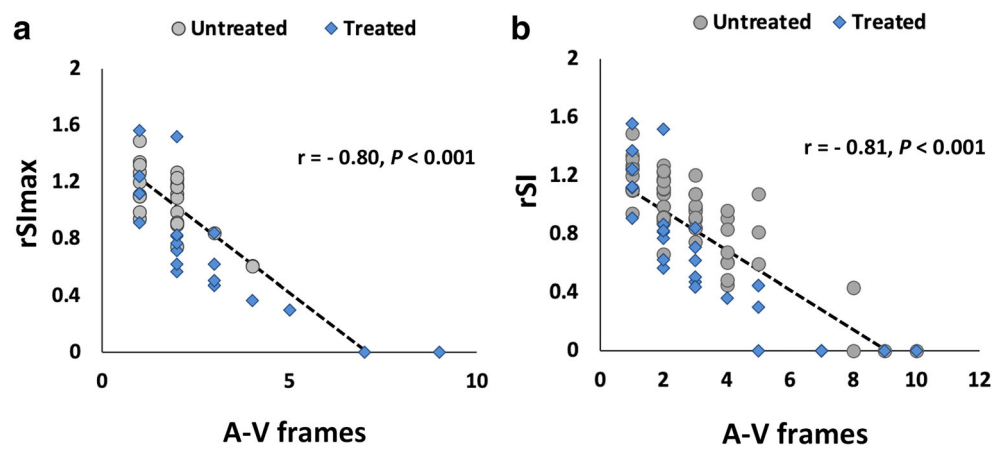


Table 2 Diagnostic performance of rSI measured by silent MRA to identify high-flow A–V shunt using DSA as a reference test

| | AUC | Cut-off value | Sensitivity | Specificity | PPV | NPV |
|--------------------|-------------------------|---------------|-------------------------|-------------------------|-------------------------|-------------------------|
| Total (n = 46) | 0.885 [0.811, 0.960] | 1.09 | 0.824 [0.558, 0.953] | 0.828 [0.709, 0.907] | 0.56 [0.353, 0.750] | 0.946 [0.842, 0.986] |
| Treated (n = 20) | 0.960 [0.882, 1.00] | 0.88 | 1 [0.517, 1] | 0.952 [0.741, 0.998] | 0.857 [0.420, 0.992] | 1 [0.800, 100] |
| Untreated (n = 26) | 0.850 [0.735, 0.965] | 1.09 | 0.818 [0.478, 0.968] | 0.767 [0.610, 0.877] | 0.474 [0.252, 0.705] | 0.943 [0.794, 0.990] |

95% confidence intervals are in brackets

DSA digital subtraction angiography, AUC area under the receiver operating characteristic curve, A–V shunt arteriovenous shunt, DSA digital subtraction angiography, MRA MR angiography, NPV negative predictive value, PPV positive predictive value, rSI ratio of signal intensity

the superior sagittal sinus and three were toward the sigmoid sinus. The corresponding A–V transit times on the DSA of these non-visualized draining veins were all more than four frames after nidal visualization (Fig. 2).

For the ROI analysis, the ICC of the measurement of rSI was 0.89 (95% CI 0.77, 0.94). The rSI_{max} of patients with high-flow A–V shunt was significantly higher than that of patients without high-flow A–V shunt (1.2 ± 0.17 vs 0.79 ± 0.37 ; $p < .001$). For draining veins with high-flow A–V shunt, rSI was significantly higher than that of draining veins without high-flow A–V shunt (1.2 ± 0.18 vs 0.74 ± 0.38 ; $p < .001$) (Fig. 3).

The rSI of each draining vein and rSI_{max} measured from silent MRA significantly correlated with the A–V transit time on DSA ($r = -0.81$, $p < .001$; $r = -0.80$, $p < .001$, respectively) (Fig. 4). This negative correlation was still significant in both patients treated ($r = -0.83$, $p < 0.001$ for rSI; $r = -0.82$, $p < 0.001$ for rSI_{max}) and those untreated ($r = -0.82$, $p < 0.001$ for rSI; $r = -0.65$, $p < 0.001$ for rSI_{max}). No significant correlation was observed between rSI_{max} and the diameter of the corresponding draining vein ($r = 0.18$, $p = 0.22$).

Table 2 shows the diagnostic performance of rSI measured from silent MRA for the determination high-flow A–V shunt in treated and untreated patients using DSA as a reference. The area under the receiver operating characteristic curve (AUC-ROC) was 0.89 (95% CI 0.81, 0.96) for all patients.

The rSI of 1.09 was set as the threshold for obtaining maximum sensitivity and specificity for high-flow A–V shunt determination. The sensitivity, specificity, positive predictive value (PPV), and negative predictive value (NPV) for high-flow A–V shunt were 82% (95% CI 55.8%, 95.3%), 82.8% (95% CI 70.9%, 90.7%), 56% (95% CI 35.3%, 75.0%), and 94.6% (95% CI 84.2%, 98.6%), respectively.

Association between the rSI on silent MRA and hemorrhage presentation

In untreated patients, the difference of the presence of high-flow A–V shunt between the hemorrhage and non-hemorrhage groups was not significant (7/12 versus 3/14, $p = 0.11$) (Table 1), nor rSI_{max} (1.1 ± 0.24 versus 1.1 ± 0.21 , $p = 0.70$); however, the draining vein with a rSI_{max} without venous ectasia was significantly observed in the hemorrhage group ($p = 0.045$) (Table 3, Fig. 5).

Discussion

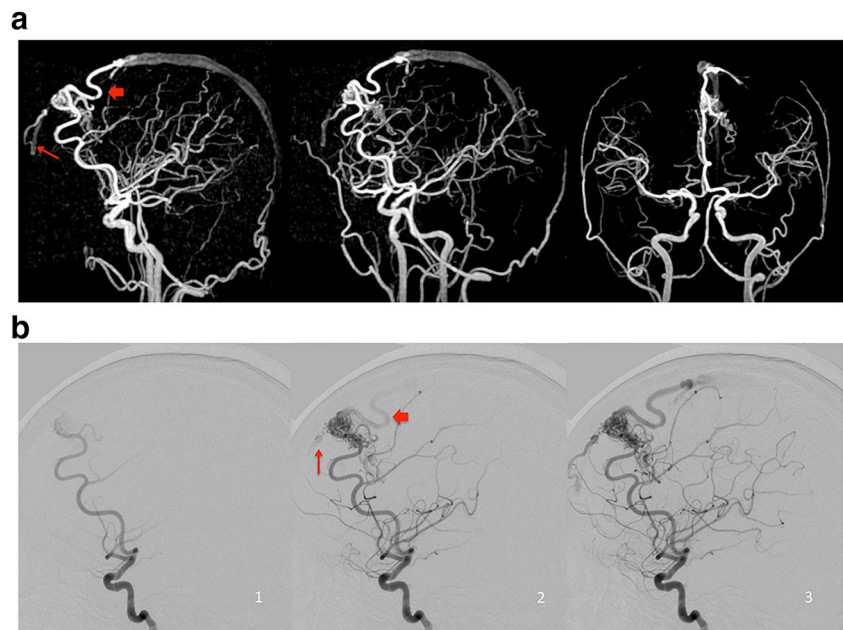
The assessment of arteriovenous (A–V) shunt was essential for risk stratification of untreated brain arteriovenous malformation (BAVM) and outcome evaluation in BAVM with endovascular or radiosurgical treatment. Therefore, an

Table 3 Silent MRA relative signal intensity in patients without treatment associated with hemorrhage presentation

| Demographics | Total (n = 26) | Hemorrhage (n = 12) | Non-hemorrhage (n = 14) | <i>p</i> value |
|--|-------------------|------------------------|----------------------------|----------------|
| rSI _{max} | 1.1 ± 0.22 | 1.1 ± 0.24 | 1.1 ± 0.21 | 0.70 |
| DV with rSI _{max} and no venous ectasia | 11 (42.3%) | 8 (66.7%) | 3 (21.4%) | 0.045 |
| DV with rSI _{max} and deep drainage | 8 (30.8%) | 5 (41.7%) | 3 (21.4%) | 0.40 |
| DV with rSI _{max} and single drainage | 9 (34.6%) | 4 (33.3%) | 5 (35.7%) | 1 |

Table entries are no. (%) or mean \pm SD. The *p* value in bold type indicates statistical significance
DV draining vein, MRA MR angiography, rSI_{max} maximum ratio of signal intensity

Fig. 5 Images of left frontal BAVM in a 28-year-old woman with hemorrhage presentation. **a** 3D MIP of Silent MR angiography showed two draining veins with no ectasia (red arrow and long arrow) toward superior sagittal sinus. **b** Lateral view of left ICA angiography. These draining veins (red arrow and long arrow) were visualized one frame after depiction of the nidus on DSA, which were classified as high-flow A–V shunt.



accurate, non-invasive imaging tool for A–V shunt analysis would facilitate the serial follow-up. The present study demonstrated that the ratio of signal intensity (rSI) measured by silent MR angiography (MRA) could be used to evaluate A–V transit time from digital subtraction angiography (DSA) in patients with BAVM. Results showed that there was a significant negative correlation between the rSI of draining veins from silent MRA and A–V transit time from DSA ($r = -0.81$, $p < .001$). Furthermore, the rSI of the draining veins from silent MRA showed excellent diagnostic performance to identify the presence of high-flow A–V shunt with a reference to DSA (area under the receiver operating characteristic curve [AUC-ROC], 0.89; $p < .001$). The current study is, to the best of our knowledge, the first study to confirm that the rSI on silent MRA is a useful non-invasive tool for identifying high-flow A–V shunt of BAVM.

Seventy-three out of all 81 draining veins (90.1%) were detected on silent MRA in our study. Comparably, previous studies have also found that a small portion of draining veins of BAVM could not be visualized on silent MRA [11–14], yet few tried to explain this phenomenon. In the current study, the non-visualized draining veins were all observed more than 4 frames after nidus visualization on DSA, suggesting that those missing draining veins in silent MRA may be a consequence of slow blood flow. A similar observation was provided in a previous study by using silent MRA to evaluate cerebrovascular diseases [15], and the authors considered that the pattern of decreasing signal intensity distally within FOV on silent MRA was probably due to signal decays with the blood T1 weighted, which has been widely recognized in conventional arterial spin label imaging [21].

Because of T1 recovery, the signal decreases with the transit time from the labeling plane. Draining veins with different transit times experience different amounts of T1 recovery in silent MRA [16, 22]. In the current study, the rSI of the draining vein on silent MRA was significantly correlated with A–V transit time on DSA. This result interpreted that a shorter A–V transit time generally resulted in less T1 recovery and higher signal intensities of draining veins. Supportive evidence has been provided by a previous study using the SI on ASL to assess the degree of arteriovenous shunting on DSA [23]. Similar to our findings, they discovered that the BAVM signal intensity on ASL correlated well with the degree of early vein opacification on DSA, which corresponded to the degree of A–V shunting. However, the study was based on the ASL map that suffers from the intrinsic low spatial resolution and could not provide the anatomical detail of BAVM vasculature. In our study, the location of ROIs over both draining veins and arteries was easy to be identified on silent MRA, which made the measurement more feasible and reliable. In addition, we selected our ROIs over each draining vein at the point closest to the nidus to reduce the confounding contributions from physiological drainage [24, 25].

The distance from the labeling plane also possibly affects the signal intensity of the draining vein. To reduce the influence of distance on the results and ensure the reliability of measurement, we applied highly standardized localization strategy and used the cavernous ICA as the denominator for the rSI reference. Furthermore, we performed similar analyses using the raw value of the SI of draining veins (see [supplementary materials](#)), without considering the influence of distance. The results were still consistent with those using rSI, which suggested that the distance from the labeling plane did not play a major role in determining the signal intensity in our study.

In the present study, the rSI of the draining veins from silent MRA showed excellent diagnostic performance to identify the presence of high-flow A–V shunt. The excellent negative predictive value and lower positive predictive value of rSI suggest that this approach may be of use in ruling out high-flow A–V shunt in patients with BAVM in follow-up examination.

In the current study, the difference of the presence of high-flow A–V shunt and the maximum rSI between hemorrhage and non-hemorrhage groups was not significant. This result is consistent with a few previous studies. Shakur et al [26] and Lin et al [25] both discovered that the transnidial time measured from QDSA was not associated with hemorrhage presentation. Furthermore, we evaluated the characteristics of draining veins with the maximum rSI and found that no venous ectasia in conjunction with the maximum rSI was significantly more observed in the hemorrhage group. Similar results were reported in a previous study on subsequent hemorrhage in children with untreated BAVM [17] which found that the combination of fast A–V shunt and no venous ectasia significantly increased future hemorrhage risk in children with BAVM. Venous ectasia might be a protective factor and reflects an adaptive mechanism whereby such dysmorphism supports either a greater efferent capacitance and/or more functional arterialization of the draining veins [27]. Further research with a larger sample size is required to prove this hypothesis.

Our study had some limitations. First, the labeling plane of silent MRA was located at the lower edge of C2 vertebral body level, which is relatively low and might reduced flow sensitivity. However, a previous study found that the perfusion effect occurred at a higher labeling plane, resulting in incomplete subtraction and affecting the accuracy of signal intensity measurement [16]. In addition, the sample size of hemorrhage analysis was relatively small. This is a preliminary study with a limited sample size and selected patients; it should be very cautious to interpret the present findings in BAVM with variable location and hemodynamic features. However, the present findings provide an evidence for the feasibility of silent MRA for the evaluation of BAVM hemodynamics in further studies.

In conclusion, the SI ratio of draining veins measured by silent MRA was correlated with arteriovenous transit time of BAVM on DSA. The rSI on silent MRA could be used as a potential biomarker of high-flow A–V shunt of BAVM. Future studies could explore silent MRA in the rupture risk assessment and outcome evaluation after interventions for BAVM, such as target embolization and radiotherapy.

Supplementary Information The online version contains supplementary material available at <https://doi.org/10.1007/s00330-021-08170-8>.

Acknowledgements Thanks are due to Doctor Juan Wei, Doctor Bing Wu, and Doctor Tao Wu of GE Healthcare for technical support.

Funding This project was supported by the Beijing Municipal Administration of Hospitals' Ascent Plan (DFL20180802) and Xuanwu Hospital Science Program for Fostering Young Scholars (QNPY2020002).

Declarations

Guarantor The scientific guarantor of this publication is Jie Lu.

Conflict of interest The authors of this manuscript declare no relationships with any companies whose products or services may be related to the subject matter of the article.

Statistics and biometry One of the authors (Chengbei Hou, PhD) has significant statistical expertise.

Informed consent Written informed consent was obtained from all subjects (patients) in this study.

Ethical approval Institutional Review Board approval was obtained.

Methodology

- retrospective
- diagnostic or prognostic study
- performed at one institution

Open Access This article is licensed under a Creative Commons Attribution 4.0 International License, which permits use, sharing, adaptation, distribution and reproduction in any medium or format, as long as you give appropriate credit to the original author(s) and the source, provide a link to the Creative Commons licence, and indicate if changes were made. The images or other third party material in this article are included in the article's Creative Commons licence, unless indicated otherwise in a credit line to the material. If material is not included in the article's Creative Commons licence and your intended use is not permitted by statutory regulation or exceeds the permitted use, you will need to obtain permission directly from the copyright holder. To view a copy of this licence, visit <http://creativecommons.org/licenses/by/4.0/>.

References

1. Stapf C, Mast H, Sciacca RR et al (2006) Predictors of hemorrhage in patients with untreated brain arteriovenous malformation. *Neurology* 66:1350–1355. <https://doi.org/10.1212/01.wnl.0000210524.68507.87>
2. Fullerton HJ, Achrol AS, Johnston SC et al (2005) Long-term hemorrhage risk in children versus adults with brain arteriovenous malformations. *Stroke* 36:2099–2104. <https://doi.org/10.1161/01.STR.0000181746.77149.2b>
3. Ogilvy CS, Stieg PE, Awad I et al (2001) Recommendations for the management of intracranial arteriovenous malformations: a statement for healthcare professionals from a special writing group of the Stroke Council, American Stroke Association. *Circulation* 103:2644–2657. <https://doi.org/10.1161/01.cir.103.21.2644>
4. Chen CJ, Ding D, Lee CC et al (2020) Stereotactic radiosurgery with versus without prior Onyx embolization for brain arteriovenous malformations. *J Neurosurg*:1–9. <https://doi.org/10.3171/2020.7.jns201731>
5. Xiaochuan H, Yuhua J, Xianli L, Hongchao Y, Yang Z, Youxiang L (2015) Targeted embolization reduces hemorrhage complications in partially embolized cerebral AVM combined with gamma knife

- surgery. *Interv Neuroradiol* 21:80–87. <https://doi.org/10.15274/inr-2014-10090>
6. Yuki I, Kim RH, Duckwiler G et al (2010) Treatment of brain arteriovenous malformations with high-flow arteriovenous fistulas: risk and complications associated with endovascular embolization in multimodality treatment. *Clinical article. J Neurosurg* 113:715–722. <https://doi.org/10.3171/2009.9.jns081588>
 7. Taeshineetanakul P, Krings T, Geibprasert S et al (2012) Angioarchitecture determines obliteration rate after radiosurgery in brain arteriovenous malformations. *Neurosurgery* 71:1071–1078; discussion 1079. <https://doi.org/10.1227/NEU.0b013e31826f79ec>
 8. Illies T, Forkert ND, Saering D et al (2012) Persistent hemodynamic changes in ruptured brain arteriovenous malformations. *Stroke* 43:2910–2915. <https://doi.org/10.1161/STROKEAHA.112.669945>
 9. Raoult H, Bannier E, Robert B, Barillot C, Schmitt P, Gauvrit JY (2014) Time-resolved spin-labeled MR angiography for the depiction of cerebral arteriovenous malformations: a comparison of techniques. *Radiology* 271:524–533. <https://doi.org/10.1148/radiol.13131252>
 10. Chang W, Loecher MW, Wu Y et al (2012) Hemodynamic changes in patients with arteriovenous malformations assessed using high-resolution 3D radial phase-contrast MR angiography. *AJNR Am J Neuroradiol* 33:1565–1572. <https://doi.org/10.3174/ajnr.A3010>
 11. Alibek S, Vogel M, Sun W et al (2014) Acoustic noise reduction in MRI using Silent Scan: an initial experience. *Diagn Interv Radiol* 20:360–363. <https://doi.org/10.5152/dir.2014.13458>
 12. Schubert T, Clark Z, Sandoval-Garcia C et al (2018) Non contrast, pseudo-continuous arterial spin labeling and accelerated 3-dimensional radial acquisition intracranial 3-dimensional magnetic resonance angiography for the detection and classification of intracranial arteriovenous shunts. *Invest Radiol* 53:80–86. <https://doi.org/10.1097/rli.0000000000000411>
 13. Tomura N, Saginoya T, Kokubun M, Horiuchi K, Watanabe Z (2019) Comparison of time-of-flight-magnetic resonance angiography from silent scan magnetic resonance angiography in depiction of arteriovenous malformation of the brain. *J Comput Assist Tomogr* 43:943–947. <https://doi.org/10.1097/rct.0000000000000935>
 14. Arai N, Akiyama T, Fujiwara K et al (2020) Silent MRA: arterial spin labeling magnetic resonant angiography with ultra-short time echo assessing cerebral arteriovenous malformation. *Neuroradiology* 62:455–461. <https://doi.org/10.1007/s00234-019-02345-3>
 15. Holdsworth SJ, Macpherson SJ, Yeom KW, Wintermark M, Zaharchuk G (2018) Clinical evaluation of silent T1-weighted MRI and silent MR angiography of the brain. *AJR Am J Roentgenol* 210:404–411. <https://doi.org/10.2214/ajr.17.18247>
 16. Wu H, Block WF, Turski PA, Mistretta CA, Johnson KM (2013) Noncontrast-enhanced three-dimensional (3D) intracranial MR angiography using pseudocontinuous arterial spin labeling and accelerated 3D radial acquisition. *Magn Reson Med* 69:708–715. <https://doi.org/10.1002/mrm.24298>
 17. Ma L, Chen XL, Chen Y, Wu CX, Ma J, Zhao YL (2017) Subsequent haemorrhage in children with untreated brain arteriovenous malformation: higher risk with unbalanced inflow and outflow angioarchitecture. *Eur Radiol* 27:2868–2876. <https://doi.org/10.1007/s00330-016-4645-3>
 18. Miyasaka Y, Yada K, Ohwada T, Kitahara T, Kurata A, Irikura K (1992) An analysis of the venous drainage system as a factor in hemorrhage from arteriovenous malformations. *J Neurosurg* 76:239–243. <https://doi.org/10.3171/jns.1992.76.2.0239>
 19. Atkinson RP, Awad IA, Batjer HH et al (2001) Reporting terminology for brain arteriovenous malformation clinical and radiographic features for use in clinical trials. *Stroke* 32:1430–1442. <https://doi.org/10.1161/01.str.32.6.1430>
 20. Cicchetti DV, Sparrow SA (1981) Developing criteria for establishing interrater reliability of specific items: applications to assessment of adaptive behavior. *Am J Ment Defic* 86:127–137
 21. Zaharchuk G, Bammer R, Straka M et al (2009) Arterial spin-label imaging in patients with normal bolus perfusion-weighted MR imaging findings: pilot identification of the borderzone sign. *Radiology* 252:797–807. <https://doi.org/10.1148/radiol.2523082018>
 22. Wolf RL, Wang J, Detre JA, Zager EL, Hurst RW (2008) Arteriovenous shunt visualization in arteriovenous malformations with arterial spin-labeling MR imaging. *AJNR Am J Neuroradiol* 29:681–687. <https://doi.org/10.3174/ajnr.A0901>
 23. Sunwoo L, Sohn CH, Lee JY et al (2015) Evaluation of the degree of arteriovenous shunting in intracranial arteriovenous malformations using pseudo-continuous arterial spin labeling magnetic resonance imaging. *Neuroradiology* 57:775–782. <https://doi.org/10.1007/s00234-015-1533-5>
 24. Brunozzi D, Hussein AE, Shakur SF et al (2018) Contrast time-density time on digital subtraction angiography correlates with cerebral arteriovenous malformation flow measured by quantitative magnetic resonance angiography, angioarchitecture, and hemorrhage. *Neurosurgery* 83:210–216. <https://doi.org/10.1093/neuros/nyx351>
 25. Lin TM, Yang HC, Lee CC et al (2019) Stasis index from hemodynamic analysis using quantitative DSA correlates with hemorrhage of supratentorial arteriovenous malformation: a cross-sectional study. *J Neurosurg* 132:1574–1582. <https://doi.org/10.3171/2019.1.jns183386>
 26. Shakur SF, Brunozzi D, Hussein AE et al (2018) Validation of cerebral arteriovenous malformation hemodynamics assessed by DSA using quantitative magnetic resonance angiography: preliminary study. *J Neurointerv Surg* 10:156–161. <https://doi.org/10.1136/neurintsurg-2017-012991>
 27. Alexander MD, Cooke DL, Nelson J et al (2015) Association between venous angioarchitectural features of sporadic brain arteriovenous malformations and intracranial hemorrhage. *AJNR Am J Neuroradiol* 36:949–952. <https://doi.org/10.3174/ajnr.A4224>

Publisher's note Springer Nature remains neutral with regard to jurisdictional claims in published maps and institutional affiliations.